Supporting Information

The binding mode of epothilone A on α,β-tubulin by electron crystallography.

James H. Nettles,[‡] Huilin Li,[•] Ben Cornett,[†] Joseph M. Krahn,[¶] James P. Snyder*[,†] and Kenneth H. Downing*[,§]

[‡]Molecular and Systems Pharmacology, Emory University, Atlanta, GA 30322; [•]Biology Department, Brookhaven National Laboratory, Upton, NY 11973, [†]Department of Chemistry, Emory University, Atlanta, GA 30322; [¶]Laboratory of Structural Biology, National Institute of Environmental Health Sciences, Research Triangle Park, North Carolina 27709; and [§]Life Sciences Division, Lawrence Berkeley National Laboratory, Berkeley, CA 94720

Epothilone A has been incorporated in zinc sulfate stabilized tubulin sheets **(Figure S-1**) that diffract electrons at a resolution below 3 Å. Herein, we describe the use of real-space molecular modeling, electron crystallographic (EC) difference mapping, and reciprocal space annealing to elucidate the atomic interactions of the drug with its tubulin receptor. Mapping reveals a model with an unexpected mode of binding that is consistent with the SAR of a wide range of epothilone analogs, but one that differs qualitatively from current pharmacophores based upon taxanes. Three dimensional coordinates and associated structure factors for the EC solution have been placed on deposit at the Protein Data Bank (*1*) (PDB; http://www.rcsb.org/pdb/)– (PDB ID - 1TVK).

JHN-jnettle@emory.edu, HL- hli@bnl.gov, JPS- jsnyder@emory.edu, KHD- khdowning@lbl.gov

Methods

Electron crystallography.

Tubulin crystals were formed as described previously. (*2*) Briefly, 25 µl of tubulin at a concentration of 10 mg/ml in 80 mM PIPES, 1 mM EGTA, 1 mM GTP, and 10 % glycerol, pH 6.8, was mixed with 50 µl 80 mM MES, 200 mM NaCl, 3 mM GTP, 1.25 mM MgSO4, 1.25 mM $ZnSO_4$, 0.025 mg/mL pepstatin, pH 5.3. The samples were incubated at 32 °C for 20 hr. Epothilone A was added at a 2:1 molar ratio of drug:tubulin-dimer and incubated at 32 °C for 15 min. For low resolution survey work in the electron microscope, samples were prepared on conventional carbon-coated grids and stained with 2% uranyl acetate aqueous solution. For high resolution EM studies, samples were embedded in a tannin-glucose mixture. Grids were held at -170 ºC and examined in a JEOL-4000 electron microscope operating at 400 kV. Electron diffraction data were recorded using a Gatan 794 2k CCD camera with typical exposures of 10 electrons per square Angstrom, low enough to avoid serious effects of radiation damage. A weak electron beam and long exposure time (40-60s) were used to minimize the vertical blooming streak in the diffraction pattern recorded with the CCD camera. Processing of diffraction data followed procedures outlined previously (*3*). Following subtraction of the radially symmetric diffuse and inelastic scattering component of the diffraction pattern and correction for geometric distortions that arise from the positioning of the CCD detector, intensities were summed in foreground and background boxes around each diffraction spot for calculation of the background-corrected spot intensity. Special care was taken to remove x-ray events from the patterns, which can produce large errors in the data. A total of 223 diffraction patterns at tilt ranges between 15°-55° were processed. **(Figure S-2**) The resolution in the direction perpendicular to the crystal plane is limited to about 4.2 Å and although resolution improves, somewhat weaker signal occurs with highly tilted specimens. Reflection intensities from individually processed diffraction patterns were merged with program Mergediff in the MRC image2000 software package (*4*). At this stage, diffraction patterns with R_{merge} larger than 28% were rejected. This removed 23 patterns, leaving a total of 200 patterns used for final merging. The measured intensities belonging to the same reciprocal space lattice

line are fitted with a smooth curve. The curve fitting program was modified so that the difference between the measured value and that predicted by the curve are printed out for further processing. Outliers with abnormally large differences were excluded in the next cycle of curve fitting. A careful trace of some of these outliers back to their original diffraction patterns indicated those spots were affected by factors such as ice crystal diffraction spots, a small patch of a second crystal, or located close to the blooming streak. The fitting was iterated 3 times until the over-all R factor between the data points and the curve no longer improved. The outlier rejection procedure improved the final R factor (25%) by 1%. The R factor from the tubulin 2D sheets is slightly higher than other comparable high resolution diffracting 2D crystals, such as bR (*5*) and LHCII. (*6*) This is because the structures of the alpha and beta subunits of the tubulin dimer are very similar, resulting in weak intensities for half of all reflections. The final 3D discrete intensity dataset was obtained by evenly sampling these lattice curves assuming a thickness of 100 Å for the 2D crystalline sheets. The dataset was converted to the standard crystallographic format, and CNS was used to randomly flag 5% of the dataset for R_{free} estimation in the subsequent crystallographic refinement process.

Model building and refinement.

Effect of resolution upon ligand omit mapping.

The refined model of αβ-tubulin complexed with Taxol (*7*) (PDB ID -1JFF) was used as the starting structure for molecular replacement modeling of the epothilone/tubulin complex. Atomic coordinate entries associated with Taxol and zinc were removed and the model was first refined in CNS1.1 (*8*) as a single rigid body with epo-A/tubulin reflection data ranging from 2.89-50 Å resolution, yielding an R factor of 0.3900. Calculations were performed with electron scatter libraries from X-PLOR(online) (*9*) and modified as Mitsuoka (5). Nucleotide parameters were obtained from the HIC-UP server (*10*). A subsequent simulated annealing of all residues with torsion angle dynamics starting at 5000 K resulted in an R_{work} of 0.3112 and R_{free} to 0.3730. To determine the effect of diffraction resolution upon ligand mapping, $2F_{obs}$-F_{calc} omit maps were calculated using the same annealed model, but at various resolution cutoffs near the high resolution limit. The graphical results shown in **Figure S-3** illustrate that the relatively small number of reflections with resolution <3.0Å were closely associated with an interpretable ligand signal. Significantly, the extension of diffraction resolution to use data to 2.89 Å results in even better density for the ligand than in the case of Taxol at 3.5 Å using experimental phases.

Effect of "shaken" protein model upon ligand omit mapping.

M-loop residues were manually rebuilt in "O" (*11*) consonant with omit maps generated using the 2.89 Å epothilone data. To remove phase bias from previous refinement, all atoms were "shaken" (*12*) by adding a random number smaller than 0.25 Å to each atom of the system and B values were uniformly set to 30. The modified protein system was subjected to torsion angle annealing starting at 5000 K using the epo-A reflection data ranging from 2.89 to 50 Å resolution. This procedure was repeated five times using different random number seeds. The resultant tubulin models differed very little from the Taxol derived predecessor except in the position of M-loop residues and orientation of His227 within the binding site. The five models were used to calculate phases and to produce $2F_{obs}$-F_{calc} "omit" maps for ligand fitting and for further protein refinement. F_{obs}-F_{calc} difference maps were also used to evaluate and correct model bias during structure determination. The new omit map from the shaken/annealed model shown in **Figures S-4** and **S-5a** displayed a more contiguous volume needed for automated ligand fitting with the same general shape and position as the map displayed in **Figure S-3a.**

NMR and NAMFIS Analysis of Epothilone B.

Given that 2.89 Å resolution is insufficient to directly define the conformation for bound epothilone A on tubulin, we adopt the principle applied in the determination of T-Taxol bound to β-tubulin, (*13*) namely that a dataset of NMR and X-ray crystal structure conformations constitutes the optimal dataset for fitting to the ligand electron crystallographic density. In the present work we have obtained solution conformations of epothilone B (**3**) from NAMFIS deconvolution (*14,15,16*) of the averaged NMR spectrum in $CDCl_3$ (*17,18*). The 400 MHz ROESY analysis of **3** delivered 42 intramolecular distances and eight 3-bond proton-proton couplings, i.e. $^3J_{HH}$. Monte Carlo Multiple Minima (MCMM) conformational analysis for **3** was performed with MacroModel 7.1 (*19*) using three separate potentials: AMBER*, MM3* and MMFFs. Only those conformations within 25 kJ/mol of the corresponding global minima were retained. The results from all three searches were combined to yield 1976 conformations. The latter pool of

structures was clustered into a smaller number of representative structures using the torsional RMS facility in XCluster 1.6 (*20*) leading to a final NAMFIS-ready dataset of 980 conformations. In addition, the conformer pool of **3** was supplemented with the X-ray crystal structure reported by Höfle et al. (*21*). The full conformer dataset and the NMR NOE/$^3J_{HH}$ data were then integrated by the NAMFIS treatment to provide a "best fit" corresponding to 17 epothilone B conformations with populations ranging from 1-14%. The fit was characterized by a reasonable sum of square distances (SSD) statistic: SSD = 53 (*14,15*). For the present purpose of locating an epothilone A conformation compatible with the EC density, the methyl group at C-12 for each of the NAMFIS conformations of **3** was replaced by hydrogen to give **2**.

Comparative evaluation of ligand binding mode and conformation.

Automated ligand fitting to the EC density was performed using the X-ligand (*22*) module in QUANTA 2000 (*23*). An X-ligand search of the 2Fo-Fc map at 0.95 sigma yielded 484 peaks of unoccupied density with the maximum peak volume located within the previously identified Taxol binding site. The unoccupied density took shape and volume compatible with both the macrocyclic ring and the side chain of epo-A (**Figure S-4 and S-5a.**). Since the X-ligand algorithm does not explore alternative ring geometries, a database representing a diversity of low energy epo-A conformations was constructed. Two epo-A conformers were obtained from structures of epo-B obtained by X-ray crystallography (2 structures) (*21*) by replacing the methyl substituent at C12 with a hydrogen and minimizing geometry with the MMFF force field in Sybyl (*24*). An additional 17 conformers came from the NAMFIS deconvolution analysis described above. The recent transfer NOE (TNOE) NMR structure of epo-A bound to tubulin (25) was also added to the database. Each of the 20 starting conformations was first rigidly, then flexibly fit with X-ligand to the EC density, the rotatable bonds explored in small increments to provide 2442 sidechain rotamers for each structure. The program oriented each torsional variant for maximal overlap of the inertia tensor matrix for the ligand with the inertia tensor matrix of the electron density and saved the top twenty fits for each starting structure. The resulting 400 orientations were evaluated graphically for consistency with various aspects of epothilone SAR. The three best fits corresponded to the X-ray structure, the TNOE NMR structure and one of the NMR/NAMFIS conformations. Since none of these forms matched the diffraction data ideally, they were modified manually to better represent the omit density and subsequently optimized with the MMFF force field in Sybyl (*24*). For the X-ray and TNOE NMR structures, this meant reorganizing the conformation of the molecule around the epoxide unit to place the three-membered ring beneath the 16-membered macrolide ring rather than outside it (**Figures 1-3, main text**). For the NAMFIS structure, the gem-dimethyl center (C4) required readjustment. The resulting three conformers were combined with the original 20 conformations and subjected to one further round of X-ligand analysis which provided a final optimal alignment of each within the omit density and the static tubulin model. From the thousands of automated fits, only two binding modes of epo-A were found to best match the experimental omit maps. These correspond to orientations with the side chain directed toward either the M-loop or His227 (**Figure S-4**). Within the 23 starting ring conformations, only those allowing near planar alignment of the side chain with the average plane of the macrolide ring could achieve such orientations. By selecting the highest scored X-ligand fit from each different conformational family, seven structures resulted; these were merged into the same protein model. The set contained both native and modified structures from X-ray, TNOE NMR, and NAMFIS analysis. Each ligand/tubulin model was refined as a rigid body in Refmac5 (*26*) and analyzed by difference mapping as illustrated in **Figure S-4**. The corresponding CCP4 maps favored models with side chains oriented toward His227 and main ring groups in contact with M-loop side chains (**S-5c** compared to **S-5d**). The modified NAMFIS conformation (**S-5b**) provided the superior match of all combinations tested. To assure ourselves that the two binding modes sampled by X-ligand did not involve an incomplete search, we tested five other plausible binding orientations of epo-A as a negative controls. All other model systems tested produced maps with similar or greater difference density than depicted in **Figures S-5c** or **S-5d.**

Final Refinement of Epothilone A bound to αβ-tubulin

The solution of epo-A bound to αβ-tubulin discussed in the main text (**Figure 1**) was derived from the complex shown in **S-5b** after localized Cartesian annealing in CNS. Epothilone parameters were derived from the HIC-UP server (*10*), and residues within 8 Å of the ligand were annealed at 5000 K while the remaining atoms were held fixed. This was repeated for 5 runs with different random number seeds. As expected, overall R factors for the shaken system changed very little during local refinement, and were not found useful as a guide to distinguishing between the resulting ligand protein complexes. Consequently, the

resulting set of models was analyzed by difference map analysis as above. The structure with the best difference map incorporated movement of Arg276 and 282 toward the ligand. Although ligand parameters were sufficiently loose to allow structural reorganization, all structures maintained shape and position consistent with the original model. Additional model systems were similarly tested and all other orientations and conformations of the ligand experienced drift toward the above structure, or moved away from the pocket.

Although all residues involved in ligand binding yield maps that give confidence in the final ligand solution, distant portions of the protein reveal densities that are not satisfied by the model and probably account for the R-factors > 0.31 Å in the current structure. Portions of the tubulin protein for which density is now available includes α35-60, not present in the previous tubulin/Taxol complex. (*7*) An overlay of the two structures shown in **Figure S-6**, illustrates that minimal change occurs between the two structures. The final model placed on deposit diverges from the structure based numbering of 1jff and uses the sequence based numbering common to biology. Like 1JFF, the alpha residues 35-60 are not included in the deposited structure due to ambiguity regarding placement. Work is ongoing to rebuild this and other portions of the tubulin model into the new data.

Tubulin Resistance against Taxol and Epothilone

Figure S-7 illustrates molecular features associated with cell lines expressing resistance bearing mutations in response to taxol or epothiloneA exposure. Discussion is in the main text.

1. H. M. Berman et al., *Nucleic Acids Research* **28**, 235 (2000).
2. E. Nogales, S. G. Wolf, S. X. Zhang, K. H. Downing, *J. Struct. Biol.* **115**, 199 (1995).
3. K. H. Downing, H. Li, *Microsc. Microanal.* **7**, 407 (2001).
4. R. A. Crowther, R. Henderson, J. M. Smith, *J. Struct. Biol.* **116**, 9 (1996).
5. K. Mitsuoka et al., *J. Mol. Biol.* **286**, 861 (1999).
6. W. Kuhlbrandt, D. N. Wang, Y. Fujiyoshi, *Nature* **367**, 614 (1994).
7. J. Lowe, H. Li, K. H. Downing, E. Nogales, *J. Mol. Biol.* **313**, 1045 (2001).
8. A. T. Brunger et al., *Acta Cryst.* **D54 (Pt 5)**, 905 (1998).
9. Peng, L.-M. *Micron* **30**, 625 (1999).
10. G. J. Kleywegt, T. A. Jones, *Acta Cryst.* **D54**, 1119 (1998).
11. T. A. Jones, J.-Y. Zou, S. W. Cowan, M. Kjelgaard, *Acta Cryst.* **D47**, 110 (1991).
12. D. E. Mcree, in *Practical Protein Crystallography*. (Academic Press, San Diego, 1993) pp. 225,273.
13. J. P. Snyder, J. H. Nettles, B. Cornett, K. H. Downing, E. Nogales, (2001) *Proc. Natl. Acad. Sci. USA* **98,** 5312-5316.
14. D.O. Cicero, G. Barbato, R. Bazzo, *J. Am. Chem. Soc.* **117**,1027-1033 (1995).
15. N. Nevins, D. Cicero, J. P. Snyder, *J. Org. Chem.* **64**, 3979-3986 (1999).
16. J. P. Snyder, Nevins, N., Cicero, D. O. and Jansen, J. *J. Am. Chem. Soc.* **122**, 724-725 (2000).
17. B. Cornett, Ph. D. Dissertation, Emory University (2002).
18. B. Cornett, A. Canales, S.-H. Kim, G. Vite, J. Jiménez-Barbero, J. P Snyder,. in preparation.
19. W. C. Still, A. Tempczyk, R. C. Hawley, T. Hendrickson, *J. Am. Chem. Soc.* **112**, 6127-6129 (1990).
20. P. S. Shenkin, D. Q. McDonald, *J. Comput. Chem.* **15**, 899-916 (1994).
21. G. Höfle *et al*., *Angew. Chem. Int. Ed.* **35**, 1567 (1996).
22. T. J. Oldfield, *Acta Cryst.* **D57**, 696 (2001).
23. Accelrys Inc. (http://www.accelrys.com/, 2001).
24. Tripos Inc. (www.tripos.com, St. Louis, 2002).
25. T. Carlomagno *et al*., *Angew. Chem. Int. Ed.* **42**, 2511 (2003).
26. Collaborative Computational Project Number 4, *Acta Cryst.* **D50**, 760 (1994).
27. N. M. Verrills *et al*., *Chem. Biol.* **10**, 597 (2003).

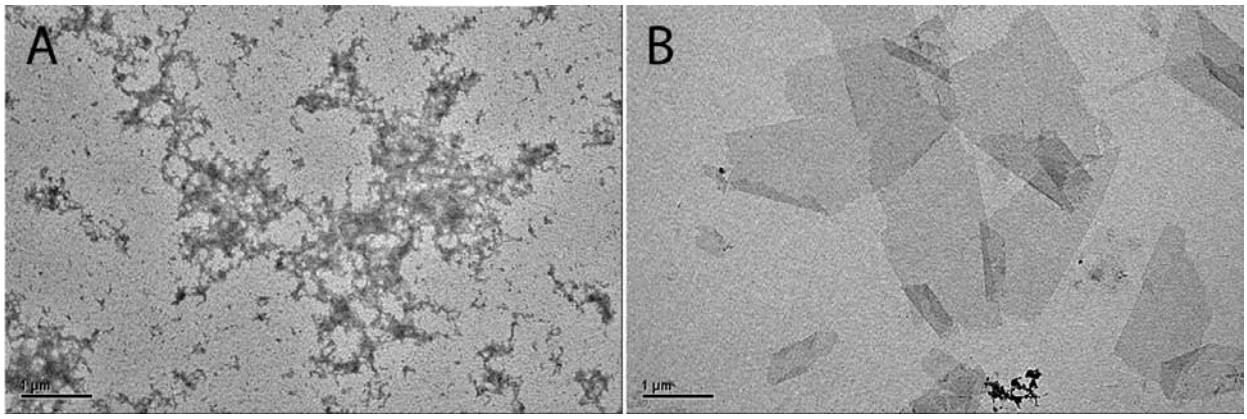

Figure S-1. Epothilone A stabilizing effect on Zn-sheets.

a) Control; no Epothilone A was added. The crystalline sheets disassembled into aggregates after a 20 min incubation on ice

b) With Epothilone A; the crystalline sheets remain intact at control conditions when exposed to the microtubule stabilizer; scale bar, 1mm.

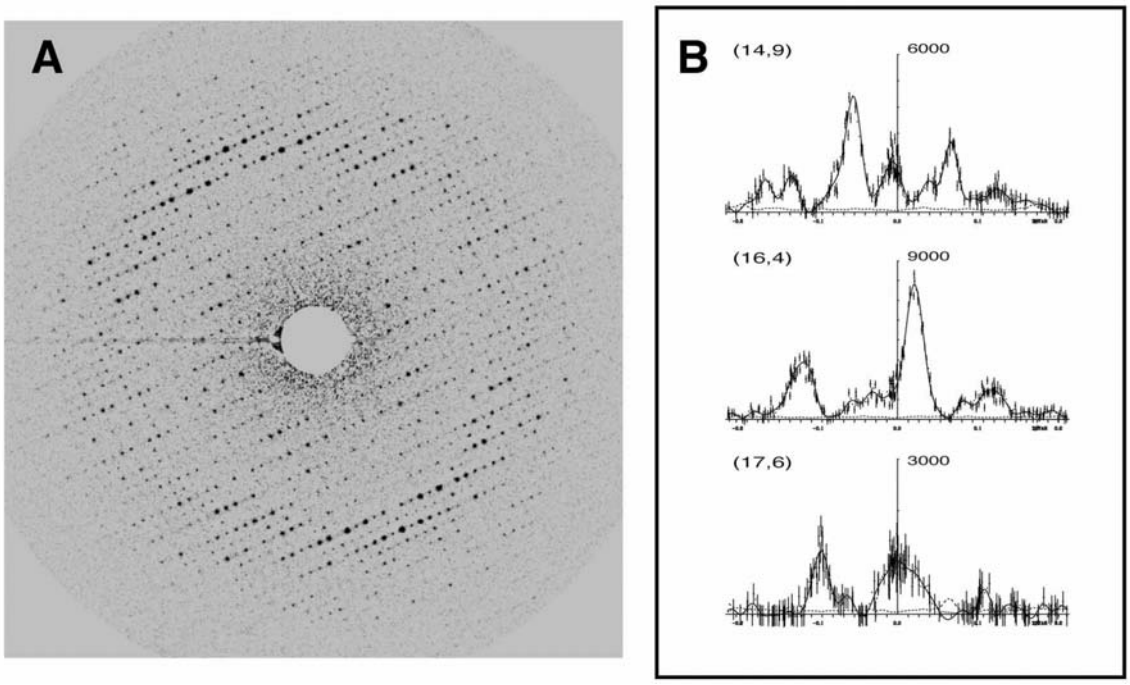

Figure S-2. Electron diffraction pattern of Zn-sheet stabilized with epothilone A.

a) Reflections extend to the edge of the image at 2.5 Å resolution.

b) Three lattice line curves. The vertical axis represents intensity in an arbitrary unit, while the horizontal axis is z*, the height of the lattice rod in reciprocal space. Note the odd numbered curve (17,6). Although the intensities are weak, the peaks are well defined because of the large number of measurements.

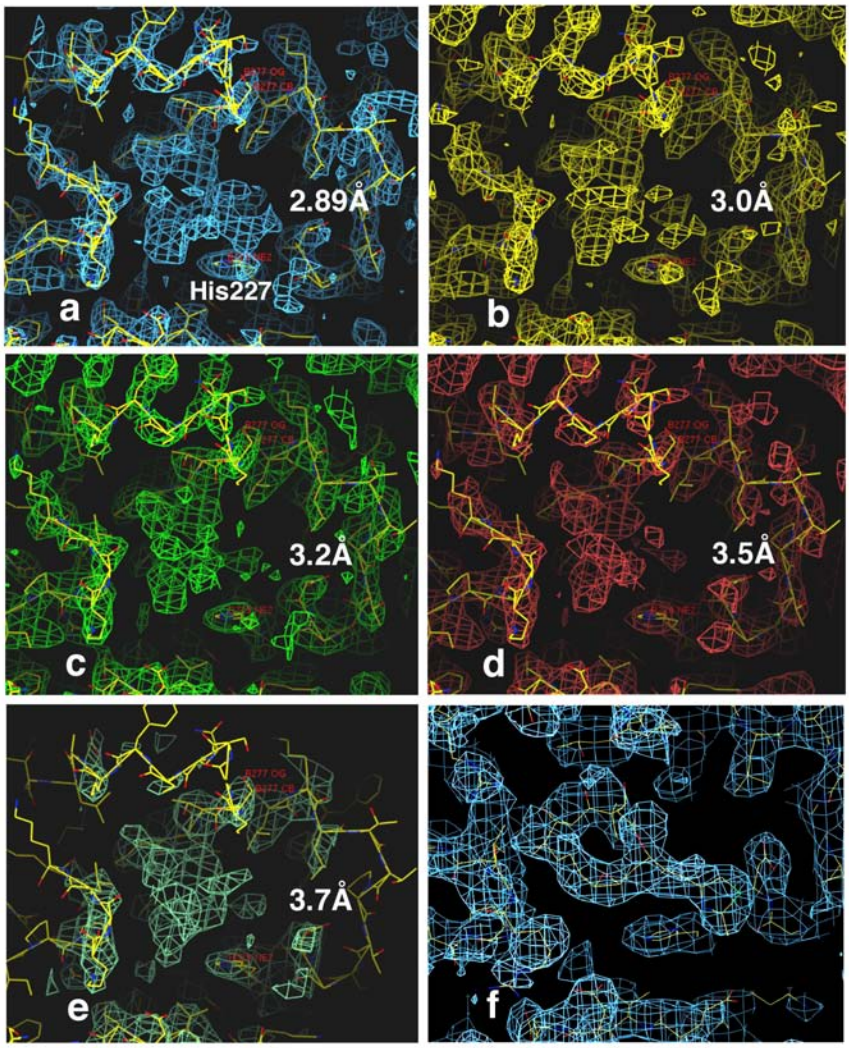

Figure S-3. The effect of diffraction resolution upon omit map projections

Frames a-e illustrate the differing results obtained as less diffraction data is included in calculation of $2F_{obs}$-F_{calc} omit maps from CNS. Each map was phased from the same high temperature simulated annealing model of the protein structure, the only change being the number of reflections used. The tubulin coordinates used for molecular replacement were obtained from the deposited structure, 1JFF, with Taxol ligand removed and B-factors uniformly set to 30 before annealing.

a) Ligand omit map using all data down to 2.89 Å. Unoccupied volumes of density above His227 approximate the shape and total spatial volume of epothilone A. Although appearing visually connected, unoccupied peaks are discontinuous at 1 sigma and become indistinguishable from noise at lower sigma levels. The discontinuous nature of this map makes it unsuitable for automated fitting.

b) Omit map calculated as in a), but with a high resolution cutoff of 3.00 Å. Considerable loss of peak density above His 227 is evident, changing the overall character of the omit pattern.

c,d,e) Omit maps calculated at 3.2 , 3.5 , and 3.7 Å cutoffs, respectively, show a systematic degradation of ligand omit signal as less high resolution data is included in the analysis.

f) A $2F_{obs}$-F_{calc} map calculated at 2.89 Å after manual fitting of the ligand and rigid refinement in Refmac (CCP4) supports the view that epo-A volume with side chain placed above His 227 is consistent with the discontinuous peaks seen in a).

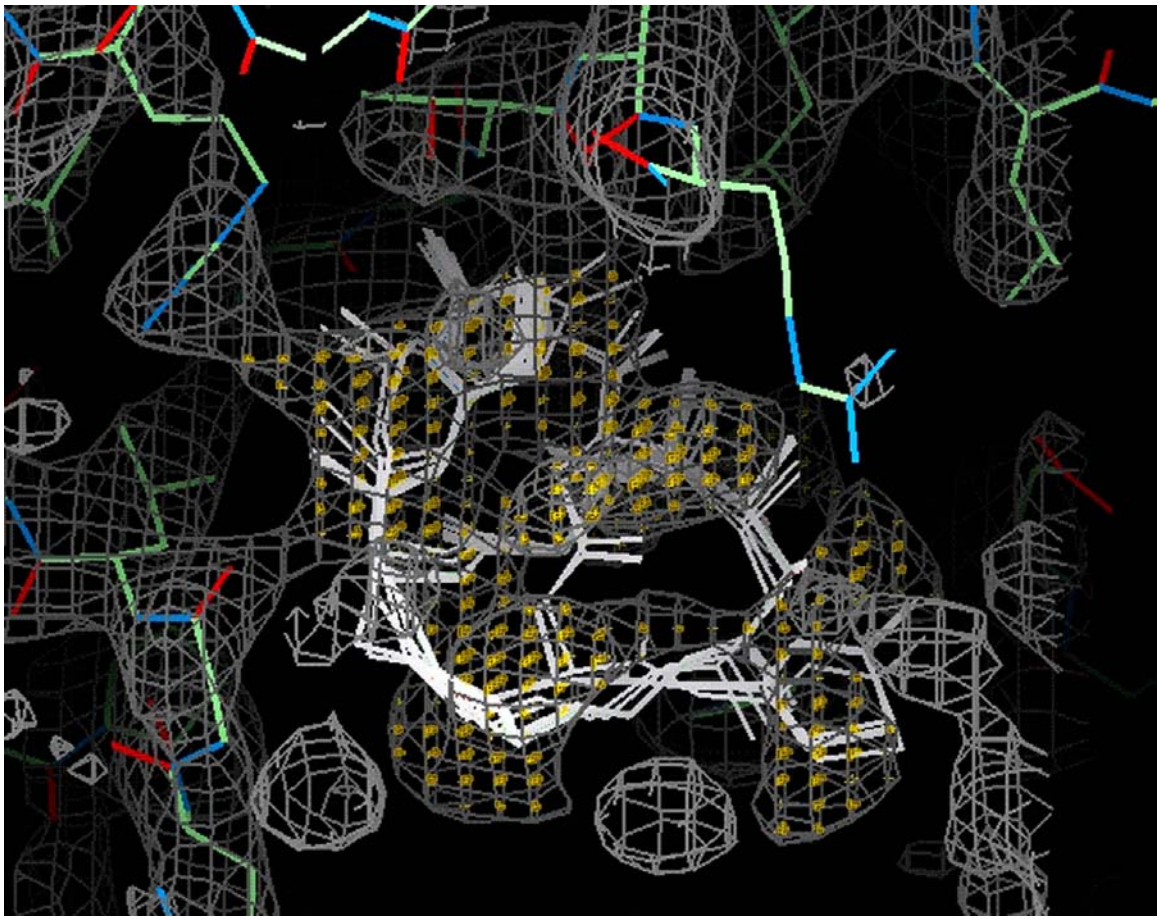

Figure S-4. The $2F_{obs}$-F_{calc} "omit" map used in the automated query

The $2F_{obs}$-F_{calc} omit map calculated in CNS with a) all reflections to 2.89 Å, and b) phases from five "shaken" high temperature annealed protein models. This omit map exhibits a similar spatial distribution and total volume by comparison with the map in Figure **SI-3a**, but it possesses a single contiguous volume suitable for automated fitting of conformational databases as described in the text. X-ligand was used to locate maximum unoccupied volume of density (highlighted in gold) and to flexibly fit epothilone rotamers from the conformational database. Only two orientations of ligand as depicted above were found to satisfy the density shape.

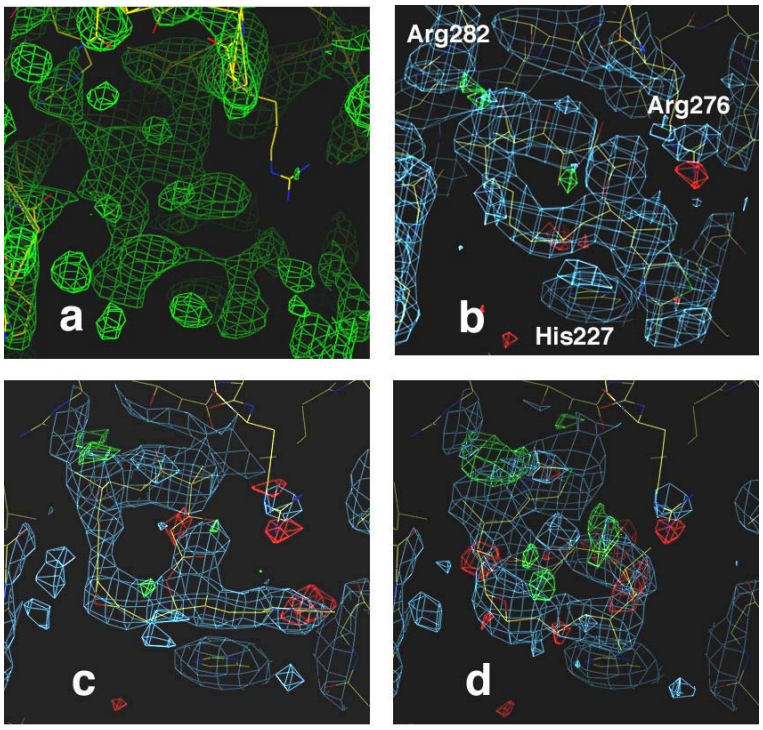

Figure S-5. The effect of varied ligand orientations and conformational models upon $2F_{obs}$-F_{calc} and F_{obs}-F_{calc} projections of the 2.89 Å diffraction data

a) The same $2F_{obs}$-F_{calc} omit map shown in **Figure SI-4** calculated in CNS with all reflections to 2.89 Å and phases from "shaken" high temperature annealed protein models. This omit map exhibits a similar spatial distribution and total volume by comparison to the map in **Figure SI-3a**, but possesses a single contiguous volume suitable for automated fitting of conformational data bases as described in text.

b-d) $2F_{obs}$-F_{calc} (sky-blue) and F_{obs}-F_{calc} (green $+3\sigma$, red -3σ) maps calculated at 2.89 Å in CCP4 using model derived phases from identical protein models, but different ligand models. In all cases, green signifies diffraction data that is not being fit by the model and red represents atomic model positions that are not supported by the diffraction data.

b) "Induced fit" variant of a NAMFIS derived, solution NMR conformation of epothilone A, automatically positioned and real space refined using X-ligand and the omit map from a). The maximum negative difference (red) in this fit is associated with a poor positioning of Arg276 away from ligand and can also be seen in c) and d). A small negative difference peak is located under the ligand, but is >1.5 Å from any model atoms. The positive difference (green), diminished upon local refinement, can also be seen near Arg282 in all maps. Atoms of residues within an 8 Å sphere of the ligand were refined by maximum likelihood in reciprocal space to the final solution pictured in **Figure 1** of the main text.

c) The TNOE NMR derived conformation of epothilone A bound to tubulin, positioned and real space refined as in b). A negative difference is associated with this epothilone model's positioning of C2, C3, and thiazole. Upon reciprocal space refinement, this ligand model shifts the side chain toward the position seen in b), but the electron density quality deteriorates.

d) Same TNOE NMR starting conformation as c), but positioned and refined by X-ligand in an "opposite" orientation that clearly puts additional negative (red) difference densities below and positive (green) density volumes within the plane of the macrocycle models used in b) and c).

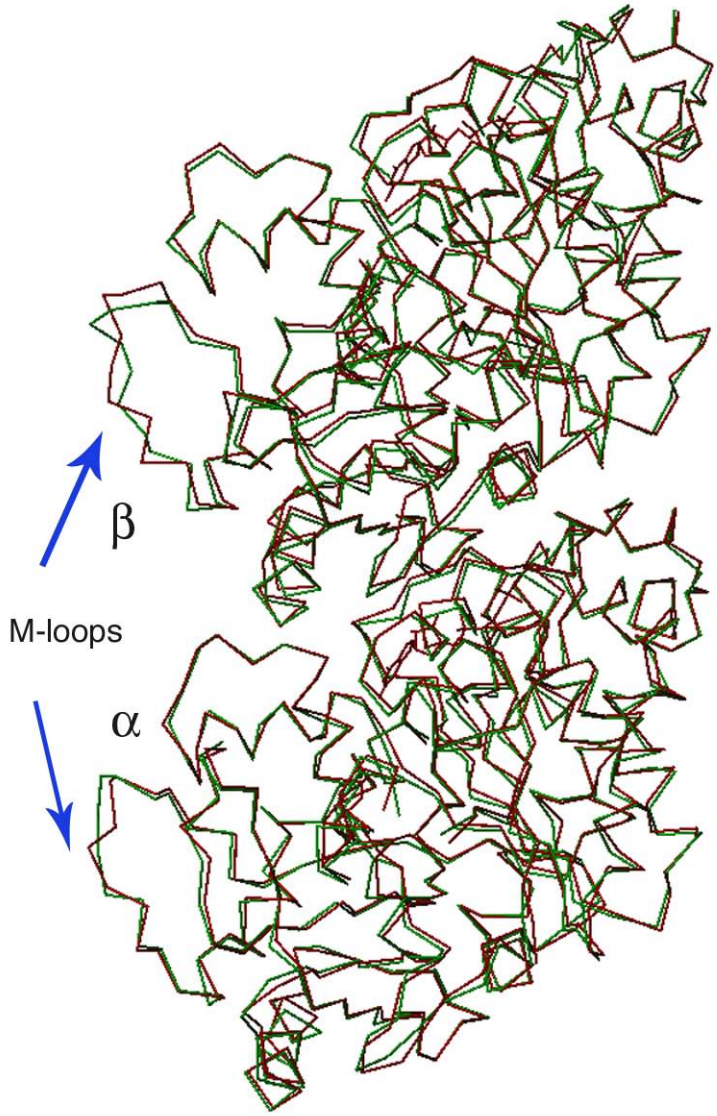

Figure S-6. C-alpha traces of deposited models of αβ-tubulin.

The backbone trace of our current model of αβ-tubulin complexed with epothilone (1TVK – red) differs very little from the previously solved taxol complex (1JFF-green) except in the M-loop region.

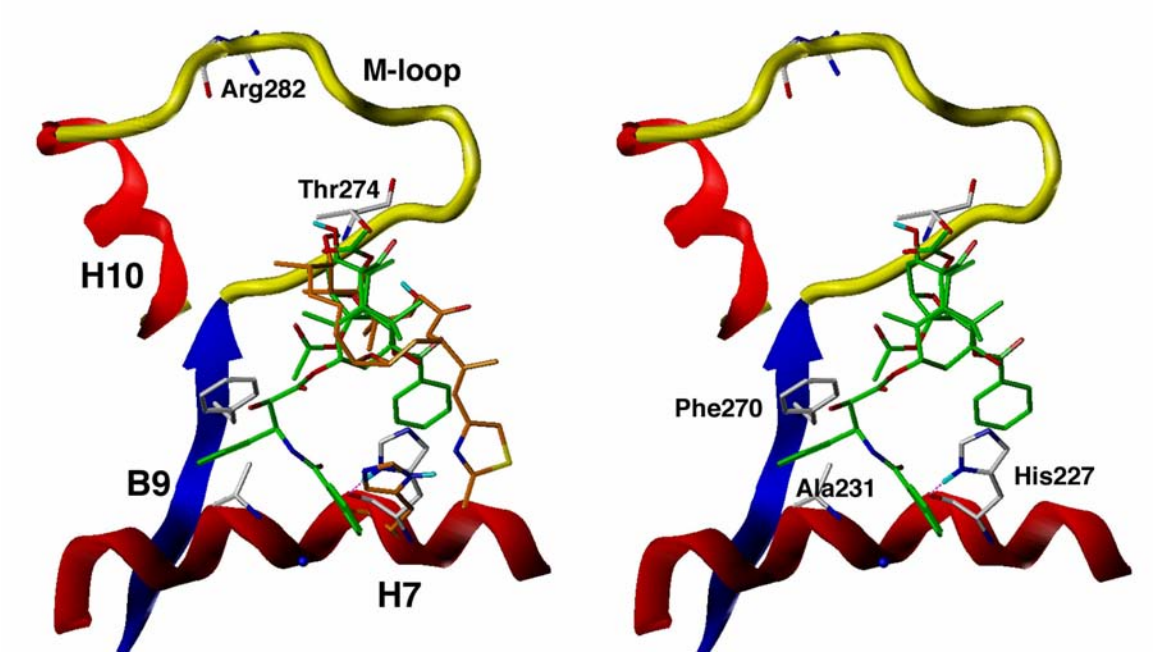

Figure S-7. Site origins of differing resistance profiles between epothilones and Taxol

T-taxol (green) in its previously published binding site *(7)* with (left) and without (right) superposition of epothilone A (orange carbons) from the current work. Unlike the extensive hydrogen bonding network illustrated for epothilone A in Figure 3 of the main text, the bound model of Taxol interacts primarily through pairing of aromatic side chains at C2 and C3' with complementary residues along the bottom of the binding site. Cells with a tubulin mutation of Phe270 to valine show 24-fold resistance to Taxol, but only 2.8-fold reduction in response to epothilone. Conversely, mutations at Arg282 and Thr274 that induce >30-fold resistance to epothilone A have a relatively small, <10 fold, affect upon Taxol activity. The M-loop positions Arg282 away from direct interaction with bound Taxol and suggests a reduced role for the hydroxyl of Thr274. The change in position of His227 (left image) associated with epothilone A's binding (orange carbons) relative to Taxol's (white carbons) is seen very clearly in the EC diffraction maps and suggests ligand specific interaction roles for this side chain. The position of Ala231 on helix 7 near His227 may be associated with the similar loss of activity shared by the two ligands upon mutation to threonine. *(27)*

Figure S-8

Structures discussed or referred to in the main text are illustrated in roughly the order mentioned. Functional groups that differ from those in epothilone A or B are highlighted in red.

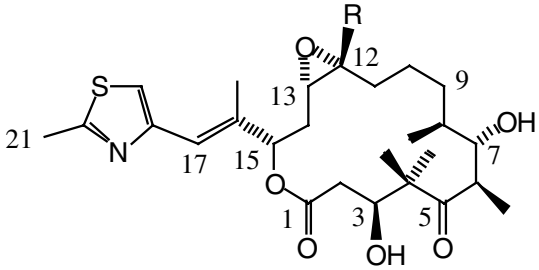

epothilone A (R = H)
epothilone B (R = Me)
epo-analog (R = hexyl)

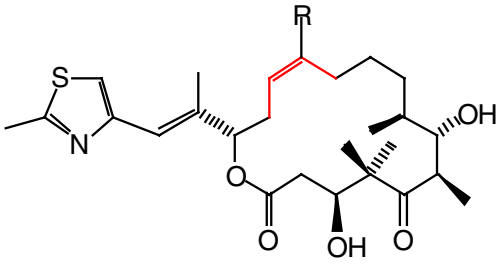

epothilone C (R = H), dEpoA
epothilone D (R = Me), dEpoB
epo-analog (R = CH2OC(O)Ph)

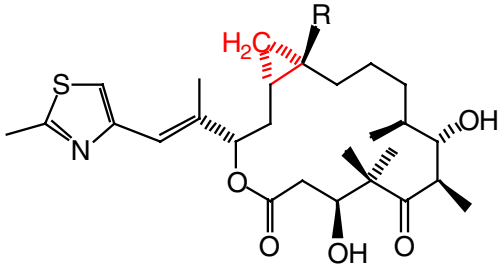

epothilone cyclopropanes

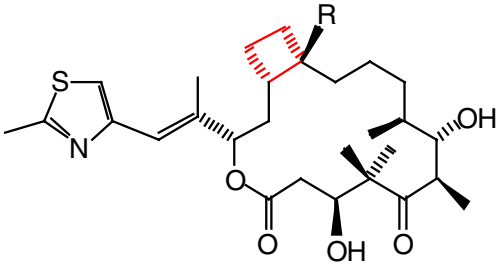

epothilone cyclobutanes

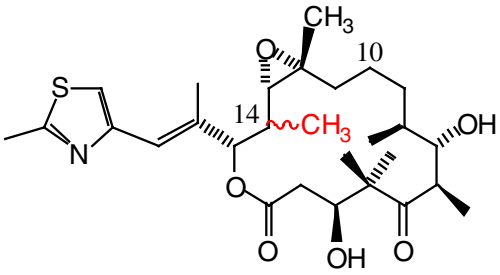

14-methyl-epothilone B isomers

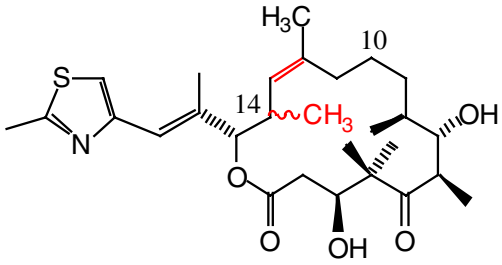

14-methyl-epothilone D isomers

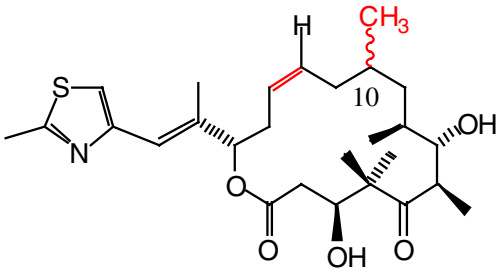

10-methyl-epothilone C isomers

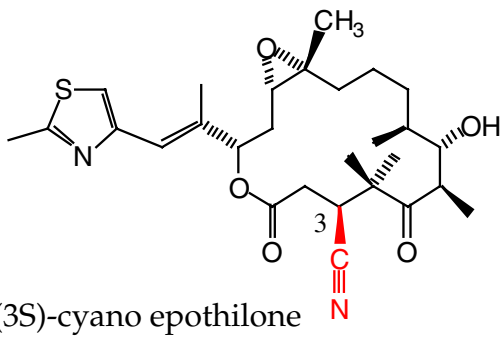

(3S)-cyano epothilone

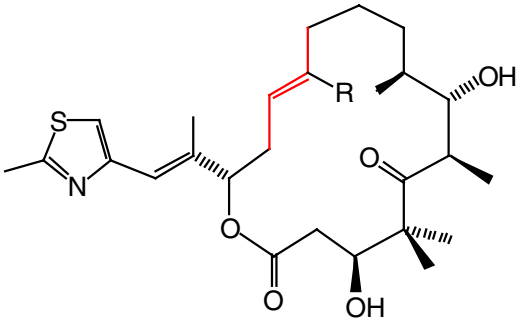

trans-epothilone C (R = H)
trans-epothilone D (R = Me)

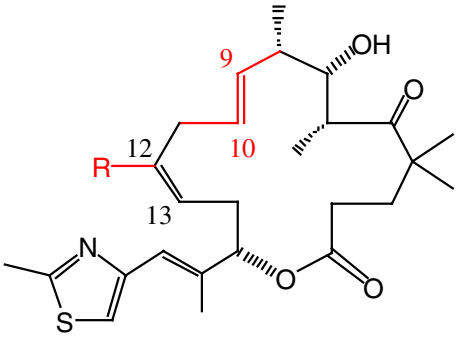

(E)-9,10-dehydro-12,13-desoxyEpoB
(R = Me); analog, R = CF_3

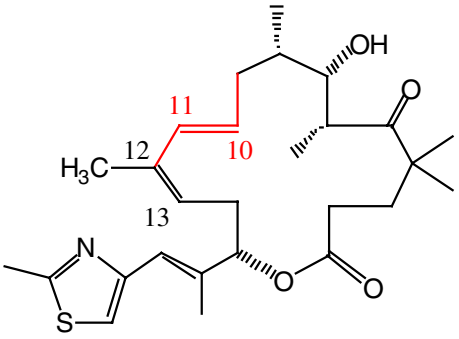

(E)-10,11-dehydro-12,13-desoxyEpoB

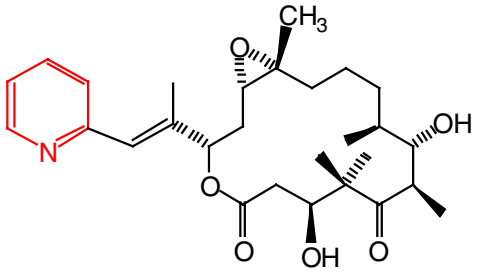

ortho-pyridine epothilone

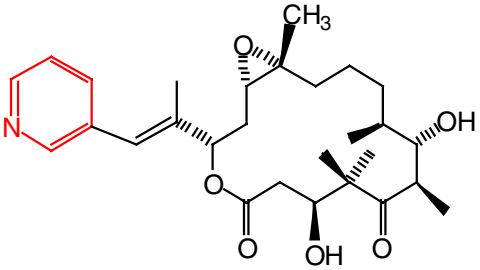

meta-pyridine epothilone

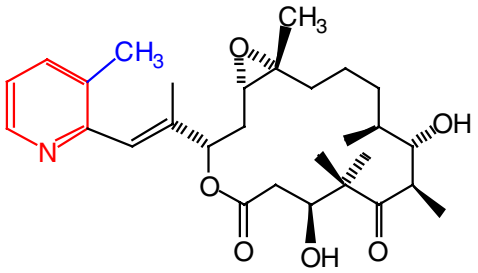

pyridine epothilone, both N & Me *ortho*

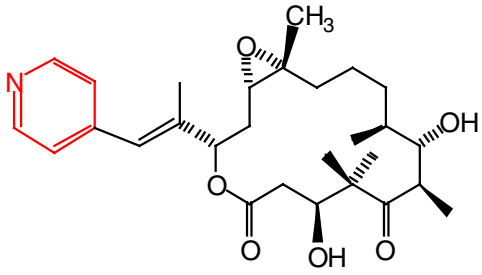

para-pyridine epothilone

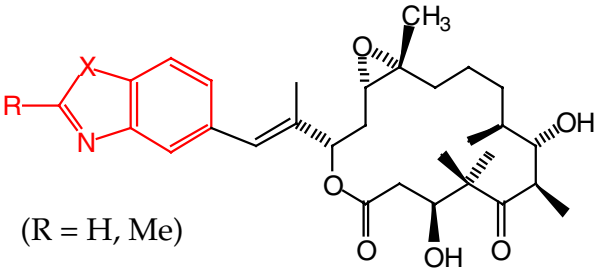

(R = H, Me)

benzo-heterocycles, X = S, NMe_2, CH=CH

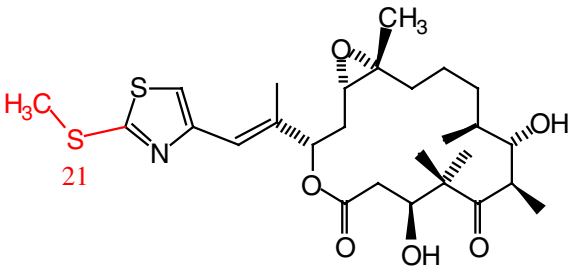

MeS_{21}-epothilone B

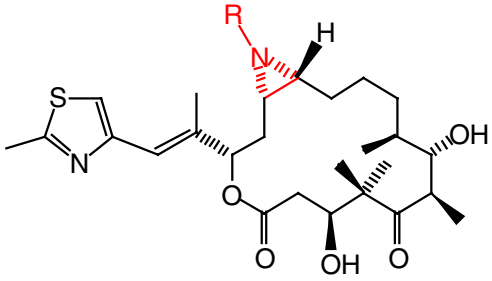

epothilone aziridines,
R = COC_6H_5, $CO_2C_6H_5$